Shock-Induced Metallization of Polystyrene Along the Principal Hugoniot Investigated by Advanced Thermal Density Functionals

R. M. N. Goshadze, V. V. Karasiev,* D. I. Mihaylov, and S. X. Hu
Laboratory for Laser Energetics, University of Rochester,
250 East River Road, Rochester, New York 14623-1299, USA
(Dated: December 5, 2022)

To date, none of the ab-initio molecular dynamics simulations of polystyrene, often used as an ablator material in inertial confinement fusion targets, with the standard ground-state exchange-correlation (XC) functional in density-functional theory can satisfactorily agree with experiments in terms of reflectivity measurements. We use recently developed thermal strongly constrained and appropriately normed Laplacian dependent meta-generalized gradient approximation XC density functional (T-SCAN-L) and thermal hybrid XC density functional (KDT0) to show that the inclusion of thermal and inhomogeneity effects is crucial for accurate prediction of structural evolution and corresponding insulator-metal transition (IMT) during shock compression. Optical reflectivity calculated as an indicator of IMT is in perfect accord with experimental data.

Introduction - The properties of polystyrene (CH) under the warm dense matter (WDM) regime, which is characterized by temperatures from tenths to several hundred electron-volts and densities from 10^{21} to 10^{25} ion/cm^3, are of uttermost importance for improving the inertial confinement fusion (ICF) target design as it is commonly used as an ablator material for both direct- and indirect-drive configurations [1–4]. In ICF implosions, the ablator material is driven to the WDM regime by shock waves [5–7] undergoing fast structural changes and related changes in physical properties. Determining the accurate thermodynamical path of the ablator material and its structural and optical properties is essential for reliable predictions on shock strength [8] and coalescence [9]. Over the years, this task has proved to be extremely arduous given that the physics of WDM can not be formulated in terms of small perturbations to accurately solvable systems at conditions challenging for conventional plasma models when both the Coulomb coupling parameter $\Gamma = e^2/(r_s k_B T)$ and the electron degeneracy parameter, also known as the reduced temperature, $t = T/T_F$ are close to unity (here $r_s = (3/(4\pi n))^{1/3}$ is the Wigner-Seitz radius, $T_F = (3\pi^2 n)^{2/3}/(2k_B)$ is the Fermi temperature; e and n are the electron charge and density, respectively) [10].

Fairly enough, CH has attracted a considerable amount of attention from theoretical, computational, and experimental standpoints [11–13]. Starting from pioneering gas-gun [14] and Nova experiments [15], the equation of state (EOS) of CH was measured on several occasions in the pressure range of 1-10 Mbar [16–19] filling the gap between gas-gun and Nova data. Overall, the results from different experimental studies align well with each other. Furthermore, in some of these studies, optical reflectivity along the principal Hugoniot was also reported. In the OMEGA experiment, as well as in the experiment at Laboratoire pour l'Utilisation des Lasers Intenses (LULI) [16] the velocity interferometer system for any reflector (VISAR) was used to detect the signal reflected by the CH shock front at the probing wavelength of 532 nm. The results from the OMEGA experiment indicated that CH remains insulating up to 1 Mbar along the principal Hugoniot, followed by a rapid jump of reflectivity to saturated value at about 0.4.

Density functional theory (DFT)-based ab-initio molecular dynamics (AIMD) simulations have already become a conventional approach for investigating WDM properties [20–23]. Even though DFT is, in principle, an exact theory, its implementation is heavily affected by the approximation of the XC functional used. Numerous approximate XC functionals have been developed for molecular and condensed matter applications. From a theoretical perspective, XC functional should be temperature-dependent; however, in practice, most of them are so-called zero-temperature or ground state approximations (GSA), meaning that they do not explicitly depend on temperature. The reason behind this is that the GSA is still reliable for many purposes at relatively low reduced temperatures when thermal XC effects are negligible and at very high temperatures when the total XC contribution becomes negligible as compared to the dominating non-interacting free-energy term. The importance of thermal XC effects is discussed in refs. [24–29]. Over the course of the last decade, several XC functionals have been employed to investigate CH principal Hugoniot and its optical properties. Wang et al. [30] performed AIMD simulation using generalized gradient approximation (GGA)-level Perdew-Wang 91 XC functional, obtaining Hugoniot data up to around 7 Mbar. In this study, both shock pressure and shock temperature were underestimated for high densities (>3 g/cm^3) as compared to recently reanalyzed OMEGA results. Another discrepancy reported by Wang is the premature jump of reflectivity followed by saturation at 0.6, which is a 50% overestimation of the OMEGA experimental value. Hu et al. carried out similar calculations [31] using PerdewBurkeErnzerhof (PBE) [32] XC functional observing stiffer behavior of shock pressure at high densi-

ties. Unlike the reflectivity saturated value discrepancy, which was easily resolved by Hu simply using the correct refraction index of unshocked CH, the discrepancies in Hugoniot data at high pressures and the premature jump in reflectivity still remain unsolved when compared to experiments. Finally, note that the calculation of optical reflectivity using HeydScuseriaErnzerhof [33] (HSE) ground-state hybrid XC functional results in only about 10% improvement near turn-on conditions and does not resolve the problem.

In this Letter, the gap between theory and experimental measurements is closed by performing AIMD simulation using recently developed T-SCAN-L thermal meta-GGA XC, which constitutes SCAN-L plus a universal thermal XC correction at the GGA level of theory [34] exploring CH principal Hugoniot in the range of temperatures between T=2200 K and 60000 K, that corresponds to reduced temperature range $0.17 < t < 0.59$, its structural properties, and reflectivity. Because of the well-known trait of non-hybrid XCs that they underestimate band gap, we calculate optical reflectivities using thermal hybrid XC (KDT0) [35] on top of T-SCAN-L-generated snapshots. Unlike T-SCAN-L, KDT0 incorporates a fraction of the exact Hartree-Fock exchange in terms of Mermin-Kohn-Sham orbitals making it more accurate (and computationally much more expensive) avoiding the band gap underestimation and corresponding overestimation of reflectivity. The inclusion of thermal and non-homogeneity effects provides perfect agreement with the abrupt turn-on of the reflectivity observed in the OMEGA experiment, indicating the accurate description of the shock-induced CH metallization. The transition of the shocked ablator material to a reflective state is driven by the dissociation of the hydrocarbon chain accompanied by the band gap closure and jump in DC conductivity.

Computational details - We perform AIMD simulations using the Vienna ab-initio simulation package (VASP) [36–38]. The VASP code is based on DFT within the framework of the Kohn-Sham scheme in which the auxiliary electron orbitals are expanded in a plane-wave basis. We use projector augmented wave (PAW) pseudopotentials with plane-wave cut-off energy of 1400 eV for all calculations in this study. For the MD runs below 2 g/cm^3 standard pseudopotentials (with a core radius of 1.3 and 1.1 bohr for C and H atoms, respectively) are used. For higher densities, we employ hard pseudopotentials with a core radius of 1.1 bohr for C and 0.8 bohr for H atoms. The transferability of the pseudopotentials to higher densities and temperatures is ensured by testing them against bare Coulomb potentials [39].

Initial structures at ambient conditions are constructed with the goal of building accurate atomistic models of syndiotactic (highly crystalline) polystyrene [40, 41]. For this purpose, we construct polystyrene chains from C_8H_8 monomers obtained from the ethylbenzene monomer (C_8H_{10}) [42] by removing two H atoms. The supercell used in calculations is orthorhombic with four 4-monomer chains with periodic boundary conditions with special attention paid to the dimensions of the cell along the polymer axis, which has been determined such that low-T geometry optimization returns stable chains. The distance between neighboring chains was determined such that ρ=1.055 g/cm^3. In order to verify the accuracy of our atomistic models, we perform calculations of electronic band gap at T = 300 K with PBE (known to underestimate $E_{\rm gap}$) and PBE0 (known to overestimate $E_{\rm gap}$) XC functionals and obtained $E_{\rm gap}^{\rm PBE} = 2.92$ eV and $E_{\rm gap}^{\rm PBE0} = 4.53$ eV respectively. Considering experimental measurement reporting $E_{\rm gap}^{\rm Exp} = 4.14$ eV [43] and a high-precision GW result $E_{\rm gap}^{GW} = 4.40$ eV [44] we conclude that our atomistic models of syndiotactic polystyrene are suitable for ab-initio simulations.

The supercell is orthorhombic with dimensions (15x17x10) $\AA$ at the ambient density and consists of 256 atoms in total (128 C and 128 H). The motivation behind using an orthorhombic supercell instead of a cubic one, for which the Baldereschi mean value is exactly known, is to accurately account for the polymeric arrangement of atoms. To sample the first Brillion zone, we tested single k-point (0.25, 0.25, 0.25) in reciprocal as well as in Cartesian coordinates and Γ-centered (2x2x2) k-mesh observing only 1% deviations in thermal and optical properties. During each MD step, ions are moved according to Newton's law and maintained in local thermodynamic equilibrium with electrons using a Nosé-Hoover thermostat. At $\rho = 2.17$ g/cm^3 and $T = 2200$ K we use MD time-step of 0.34 fs, and for other conditions, this value is scaled according to density and temperature $\sim \rho^{-1/3}T^{-1/2}$. The density of CH is controlled by isotropic compression of the supercell by adiabatically shrinking the volume. We use the number of bands changing from 350 to 1800 for Hugoniot calculations, while for optics calculations, we increase it by a factor of 3. By performing the path integral molecular dynamics (PIMD) simulations, we verify that ionic quantum effects are negligible for EOS and optical variables.

Results and discussion - EOS of shocked material just behind the shock front satisfies the Rankine-Hugoniot equation

$$E_1 - E_0 + \frac{1}{2}(P_1 + P_0)\left(\frac{1}{\rho_1} - \frac{1}{\rho_0}\right) = 0 \qquad (1)$$

where the subscripts "0" and "1" stand for unshocked and shocked sides, respectively. The unshocked side of the ablator (CH) is in ambient conditions. At ambient conditions (T = 300 K and $\rho = 1.055$ g/cm^3), the pressure, P_0, can be well approximated by zero since it is orders of magnitude lower than the pressure at around $\sim 10^3$ K, or the lowest temperature at which we search for Hugoniot point. Based on the results from our AIMD calculations, E_0 is set to be -93 kJ/g.

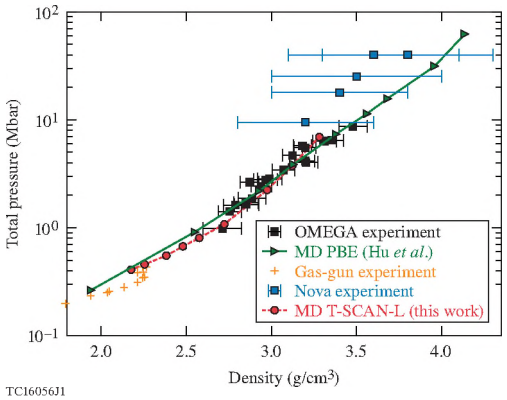

FIG. 1: CH pressure as a function of density along the principal Hugoniot. The T-SCAN-L results (red circles) are compared with PBE calculations by Hu et al. (green triangles) [31], the Nova experiment (blue rectangles) [15], gas-gun experiment (yellow crosses) [14], and the OMEGA experiment [45] based on latest quartz EOS (black rectangles).

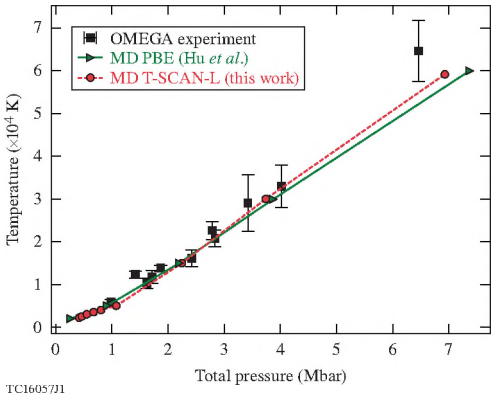

FIG. 2: CH temperature as a function of pressure along the principal Hugoniot. The T-SCAN-L results (red circles) are compared with PBE calculations by Hu et al. (green triangles) [31], and the OMEGA experiment [45] based on latest quartz EOS (black rectangles).

For given temperature T, we change density ρ_1 to obtain internal energy density E_1 and pressure P_1 satisfying equation (1). For the conditions where the internal structure of CH is still present (up to 15000 K), we change the density with only 0.05 g/cm^3 increment during each adiabatic compression step. Above that, no structural relaxation is needed since the CH is already completely dissociated.

Fig. 1 shows the comparison between various experimental and theoretical studies of principal Hugoniot on the pressure-density plane. As we see, both PBE (green triangles) [31] and T-SCAN-L (red circles) AIMD calculations overestimate shock pressure as compared with gas-gun [14] experiment (yellow crosses) below 1 Mbar. In the middle-pressure range (1-10 Mbar), T-SCAN-L shows concave behavior opposing more linear PBE results. Apart from using higher-rung XC functional with explicit temperature dependence, this change might also be associated with the proper treatment of structural characteristics of shocked CH. We carefully run structural relaxation until no structure remains, observing melting/dissociation exactly at these middle-range pressures, as will be discussed later. Note that each of the last two updates of quartz EOS data [18, 45] made pressures from the OMEGA experiment 2-3% stiffer, but at the merging point (around 10 Mbar), the gap between Nova and OMEGA values is still present. Despite possible radiation preheat issues and larger error bars of NOVA data compared to the OMEGA experiment, the interpolation curve of Hugoniot points, which shows stiffer behavior than previous studies, might motivate further high-pressure (above 10 Mbar) experimental and theoretical work.

In Fig. 2, the predicted shock temperature is plotted as a function of pressure from AIMD calculations (red circles) that is compared with AIMD results using PBE XC functional by Hu et al. (green triangles) [31], and with OMEGA experiment (black squares) [45]. At lower pressures, both PBE and OMEGA calculations agree well with our T-SCAN-L AIMD results. The more interesting behavior is observed at higher pressures. Starting from 3.8 Mbar, we see that the shock temperature predicted by T-SCAN-L AIMD starts to deviate from PBE results. In previous studies, this mismatch was attributed to uncertainties in quartz's temperature at such high pressures, but our results show that inhomogeneity and thermal effects might also lead to removing the discrepancy.

When CH is under shock compression, chemical

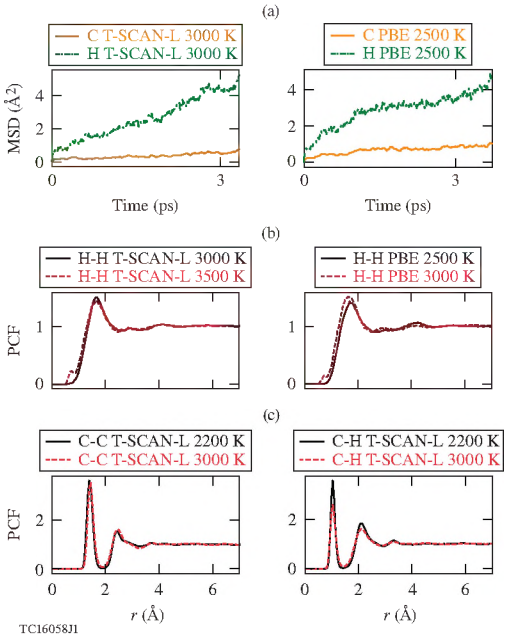

FIG. 3: (a) MSDs of carbon and hydrogen atoms as predicted by T-SCAN-L and PBE at 3000 K and 2500 K, respectively. (b) PCFs of H-H bond predicted by T-SCAN-L and PBE. (c) PCFs of C-C and C-H bonds at 2200 K and 3000 K.

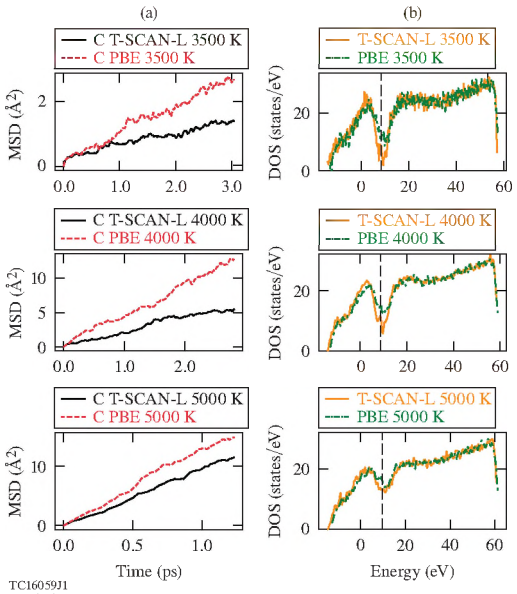

FIG. 4: (a) Comparison of MSDs predicted by PBE vs. T-SCAN-L XC functionals. (b) comparison of corresponding DOS in the temperature range of 3500-5000 K.

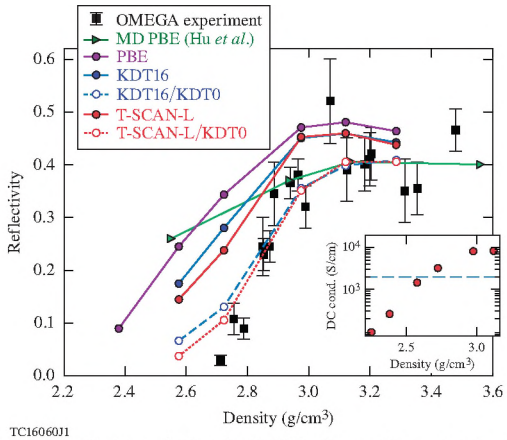

FIG. 5: Reflectivity of shocked CH along the principal Hugoniot at 532 nm VISAR light. T-SCAN-L/KDT0 (red empty circles), T-SCAN-L (red filled circles), KDT16/KDT0 (blue empty circles), KDT16 (blue filled circles), OMEGA experiment (black squares) [18], PBE calculations by Hu et al. with $n_0 = 1.74$ (green triangles) [31], PBE reflectivity along the T-SCAN-L Hugoniot (purple circles). The inset shows the corresponding jump in DC conductivity, where the blue dashed line is at 2000 S/m - the formal boundary between insulating and conductive states.

decomposition due to shock gives rise to IMT of ablator material as discussed in earlier works [30, 31]. Therefore, in order to fully understand the dynamics of transition to conducting state along the principal Hugoniot, it is essential to carefully examine structural changes. For this purpose, we begin the simulation from a perfectly condensed hydrocarbon chain and relax the supercell all the way up to 15000 K, where almost no chemical structure is present. The first important change in the polymeric structure is the dissociation of hydrogen atoms from the hydrocarbon chain. This behavior is indicated in the increasing gap between mean square displacement (MSD) functions of hydrogen and carbon atoms as shown in Fig. 3 (a). This observation is further justified with pair correlation functions (PCF). We see that from 2200 K to 3000 K, no apparent change occurs in C-C PCF [Fig. 3 (c)], while both peaks in C-H PCF drop significantly. At slightly higher temperatures, the emergence of the first peak in H-H PCF shown in Fig. 3 (b) indicates the formation of molecular hydrogen. It should be stressed here that the exact same behavior is observed in PBE-based simulations, but yet 500 K earlier. Moving up with temperature, we observe the degradation of the carbon skeleton, but under all conditions, the carbon atoms in PBE simulations show higher mobility level as compared to T-SCAN-L simulations [Fig. 4 (a)]. The degradation/dissociation continues up to 15000 K, which corresponds to 2.97 g/cm^3 and 2.24 Mbar along the principal Hugoniot.

Now we turn our attention to the optical properties and make a connection to the stages of structural decomposition described above. We perform optical calculations within the Kubo-Greenwood formalism, obtaining CH reflectivity by averaging over the uncorrelated snapshots of ionic configurations from our AIMD simulations. The details of the process that we follow can be found in [31]. The essence of the approach is to construct velocity dipole matrix elements from Mermin-Kohn-Sham orbitals and use them to obtain frequency-dependent Onsager coefficients. The delta function in this calculation is approximated by the Gaussian with a width of 0.5. Reflectivity is defined as

$$R(w) = \frac{[n(w) - n_0]^2 + k(w)^2}{[n(w) + n_0]^2 + k(w)^2} \qquad (2)$$

where $n(w)$ and $k(w)$ are frequency-dependent real and imaginary parts of refraction index respectively, and n_0 is the refraction index of unshocked CH, which is set to be 1.59 based on the experimental value [46]. We use an experimental refraction index to avoid double error (error from ambient and shocked state calculations) cancellation and exclusively concentrate on the shocked state. The comparison of the results from our calculations with the OMEGA experiment and PBE-based AIMD study [31] is shown in Fig. 5. We see that the reflectivity turn-on point is shifted to higher pressures and the jump is much sharper, making it in perfect agreement with the OMEGA experiment. By separately plotting the results obtained by T-SCAN-L (red filled circles) and by KDT0 on top of T-SCAN-L-generated ionic configurations (red empty circles) in Fig. 5, we demonstrate that the improved results are the consequence of not only accurate ionic configurations but also accurate electronic structure calculations. Also, note that the reflectivity starts rapid jump and reaches saturated value with carbon skeleton

degradation. There are several factors that contribute to this enhancement. Foremost, our PBE calculations (corresponding to purple dots in Fig. 5. where we used PBE for MD run as well as for Kubo-Greenwood calculations but along the T-SCAN-L-calculated Hugoniot conditions) show that it underestimates the drop in density of states (DOS) as compared to T-SCAN-L at exact the same conditions. This argument is summarized in Fig. 4 (b) by providing a comparison of DOS in the temperature range from 3500 K to 5000 K, along the principal Hugoniot. We see that at all conditions, T-SCAN-L predicts a deeper drop in DOS, indicating fewer available states near the Fermi energy level, which is the reason for the observed lower optical reflectivity and DC conductivity in both AIMD calculations and experiments during the CH metallization process. The second aspect is the shift in Hugoniot data. At lower densities (below 3 g/cm^3), T-SCAN-L gives lower Hugoniot pressures as compared to PBE calculations. As a result, the Hugoniot points at a fixed density predicted by T-SCAN-L have much less molecular dissociation and consequently exhibit a deeper drop in DOS, leading to smaller reflectivity. Lastly, we performed optical calculations using PBE XC functional with snapshots from MD runs of T-SCAN-L and found that even in this case, PBE overestimates reflectivity by ∼3%, in comparison to the case of T-SCAN-L for both procedures (i.e., T-SCAN-L for MD and T-SCAN-L for Kubo-Greenwood calculations).

To further investigate the underlying nature of this remarkable improvement, we also test thermal GGA level XC functional, Karasiev-Dufty-Trickey (KDT16) [47]. As in the case of T-SCAN-L, we also perform KDT0 calculations on top of KDT16-generated snapshots (KDT16/KDT0). KDT16 predicts the Hugoniot as accurately as T-SCAN-L. However, as shown in Fig. 5, KDT16 (blue filled circles), as well as KDT16/KDT0 (blue empty circles), reflectivities are higher before saturation compared to T-SCAN-L (red filled circles) and T-SCAN-L/KDT0 (red empty circles) values, respectively. As PBE and KDT16 have the same non-thermal behavior and KDT16 and T-SCAN-L have the same temperature dependence, we can conclude that the incorporation of both, thermal and meta-GGA inhomogeneity effects along with the fraction of exact Hartree-Fock exchange via KDT0, is essential to completely resolve the discrepancy.

Summary - In summary, we performed AIMD simulations for shocked CH in the framework of DFT using meta-GGA level thermal XC functional - T-SCAN-L comparing it with previous experimental and theoretical works as well as our PBE calculations. We obtained principal Hugoniot data up to ∼ 7Mbar and investigated its structural and optical properties. Both shock-pressure and shock-temperature predicted by T-SCAN-L show stiffer behavior compared to PBE calculations making it in better agreement with experiments. Moreover, it was demonstrated that the inclusion of thermal and inhomogeneity effects via advanced thermal XC functional better describes the shock-induced dissociation of CH. Namely, in T-SCAN-L simulations, hydrogen dissociation, formation of molecular hydrogen, and melting of carbon skeleton are observed at higher temperatures compared to PBE. Finally, the disagreement of PBE-predicted reflectivity with experimental results during CH metallization, which is caused by early melting/dissociation and corresponding band gap closure, is completely resolved by employing KDT0 XC functional on top of T-SCAN-L-generated snapshots.

Acknowledgements- This report was prepared as an account of work sponsored by an agency of the U.S. Government. Neither the U.S. Government nor any agency thereof, nor any of their employees, makes any warranty, express or implied, or assumes any legal liability or responsibility for the accuracy, completeness, or usefulness of any information, apparatus, product, or process disclosed, or represents that its use would not infringe privately owned rights. Reference herein to any specific commercial product, process, or service by trade name, trademark, manufacturer, or otherwise does not necessarily constitute or imply its endorsement, recommendation, or favoring by the U.S. Government or any agency thereof. The views and opinions of authors expressed herein do not necessarily state or reflect those of the U.S. Government or any agency thereof.

This material is based upon work supported by the Department of Energy National Nuclear Security Administration under Award Number DE-NA0003856 and US National Science Foundation PHY Grant No. 1802964.

* Corresponding Author: vkarasev@lle.rochester.edu

[1] S. W. Haan et al., Physics of Plasmas **18**, 051001 (2011).
[2] D. D. Meyerhofer et al., Nucl. Fusion **51**, 053010 (2011).
[3] Betti, R., Hurricane, O., Nature Phys. **12**, 435448 (2016).
[4] R. S. Craxton *et al.*, Physics of Plasmas **22**, 110501 (2015).
[5] B. A. Hammel, S. W. Haan, D. S. Clark, M. J. Edwards, S. H. Langer, M. M. Marinak, M. V. Patel, J. D. Salmonson, and H. A. Scott, High Energy Density Phys. **6**, 171 (2011).
[6] T. R. Boehly *et al.*, Physics of Plasmas. **18**, 092706 (2011).
[7] S. Atzeni *et al.*, Nucl. Fusion **54**, 054008 (2014).
[8] H. F. Robey, J. D. Moody, P. M. Celliers, J. S. Ross, J. Ralph, S. LePape *et al.*, Phys. Rev. Lett. **111**, 065003 (2013).
[9] T. R. Boehly, V. N. Goncharov, W. Seka, M. A. Barrios, P. M. Celliers, D. G. Hicks, G. W. Collins, S. X. Hu, J. A. Marozas, and D. D. Meyerhofer, Phys. Rev. Lett. **106**, 195005 (2011).
[10] Jeff Colvin and Jon Larsen, *Extreme Physics* (Cambridge University Press, 2014).

[11] G. Huser, V. Recoules, N. Ozaki, T. Sano, Y. Sakawa, G. Salin, B. Albertazzi, K. Miyanishi, and R. Kodama, Phys. Rev. E **92**, 063108 (2015).

[12] P. Colin-Lalu, V. Recoules, G. Salin, T. Plisson, E. Brambrink, T. Vinci, R. Bolis, and G. Huser, Phys. Rev. E **94**, 023204 (2016).

[13] G. Huser, N. Ozaki, P. Colin-Lalu, V. Recoules, T. Sano, Y. Sakawa, K. Miyanishi, and R. Kodama, Physics of Plasmas **25**, 052706 (2018).

[14] Edited by S. P. Marsh, *LASL Shock Hugoniot Data* (Los Alamos Series on Dynamic Material Properties, University of California Press, Berkeley, CA, 1980, ????).

[15] R. Cauble, L. B. Da Silva, T. S. Perry, D. R. Bach, K. S. Budil, P. Celliers, G. W. Collins, A. Ng, T. W. Barbee, Jr., B. A. Hammel, N. C. Holmes, J. D. Kilkenny, R. J. Wallace, G. Chiu, and N. C. Woolsey, Phys. Plasmas **4**, 1857 (1997).

[16] M. Koenig, F. Philippe, A. Benuzzi-Mounaix, D. Batani, M. Tomasini, E. Henry, and T. Hall, Phys. Plasmas **10**, 3026 (2003).

[17] S. Hamel, L. X. Benedict, P. M. Celliers, M. A. Barrios, T. R. Boehly, G. W. Collins, T. Doppner, J. H. Eggert, D. R. Farley, D. G. Hicks, J. L. Kline, A. Lazicki, S. LePape, A. J. Mackinnon, J. D. Moody, H. F. Robey, E. Schwegler, and P. A. Sterne, Phys. Rev. B **86**, 094113 (2012).

[18] M. A. Barrios, D. G. Hicks, T. R. Boehly, D. E. Fratanduono, J. H. Eggert, P. M. Celliers, G. W. Collins, and D. D. Meyerhofer, Phys. Plasmas **17**, 056307 (2010).

[19] N. Ozaki *et al.*, Phys. Plasmas **16**, 062702 (2009).

[20] Shuai Zhang and S.X. Hu, Phys. Rev. Lett. **125**, 105001 (2020).

[21] J. Hinz, V. V. Karasiev, S. X. Hu, M. Zaghoo, D. Mejía-Rodríguez, S. B. Trickey, and L. Calderín, Phys. Rev. Research **2**, 032065(R) (2020).

[22] Michael P. Desjarlais, Christian R. Scullard, Lorin X. Benedict, Heather D. Whitley, and Ronald Redmer, Phys. Rev. E **95**, 033203 (2017).

[23] R. Paul, S.X. Hu, and V.V. Karasiev, Phys. Rev. Lett. **122**, 125701 (2019).

[24] V. V. Karasiev, L. Calderín, and S. B. Trickey, Phys. Rev. E **93(6)**, 063207 (2016).

[25] V. V. Karasiev, S. X. Hu, M. Zaghoo, and T. R. Boehly, Phys. Rev. B **99**, 214110 (2019).

[26] Kushal Ramakrishna, Tobias Dornheim, and Jan Vorberger, Phys. Rev. B **101**, 195129 (2020).

[27] M. W. C. Dharma-wardana, Computation **4** (2016), ISSN 2079-3197.

[28] M. W. C. Dharma-wardana, J. Phys.: Conf. Ser. **442**, 012030 (2013).

[29] Travis Sjostrom and Jrme Daligault, Phys. Rev. B **90**, 155109 (2014).

[30] Cong Wang, Xian-Tu He, and Ping Zhang, Physics of Plasmas **18**, 082707 (2011).

[31] S. X. Hu, T. R. Boehly, and L. A. Collins, Phys. Rev. E **89**, 063104 (2014).

[32] John P. Perdew, K. Burke, and M. Ernzerhof, Phys. Rev. Lett. **77**, 3865 (1996).

[33] N. J. Hartley *et al.*, Matter Radiat. Extremes **5**, 028401 (2020).

[34] V. V. Karasiev, D. I. Mihaylov, and S. X. Hu, Phys. Rev. B **105**, L081109 (2022).

[35] D. I. Mihaylov, V. V. Karasiev, and S. X. Hu, Phys. Rev. B **101**, 245141 (2020).

[36] G. Kresse and J. Hafner, Phys. Rev. B **47**, 558 (1993).

[37] G. Kresse and J. Hafner, Phys. Rev. B **49**, 14251 (1994).

[38] G. Kresse and J. Furthmuller, Phys. Rev. B **54**, 11169 (1996).

[39] Shuai Zhang et al., Phys. Rev. E **106**, 045207 (2022).

[40] O. Greis, Y. Xu, T. Asano, and J. Petermann, Polymer **30**, 590 (1989).

[41] Yozo Chatani, Yukio Shimane, Yuko Inoue, Tomoko Inagaki, Tsutomu Ishioka, Toshikazu Ijitsu, and Toshimitsu Yukinari, Polymer **33**, 488 (1992).

[42] Dmitry S Yufit, Acta Crystallographica Section C: Crystal Structure Communications **69**, 273 (2013).

[43] S. A. Saqan, A. S. Ayesh, A. M. Zihlif, E. Martuscelli, and G. Ragosta, Polymer Testing **23**, 739 (2004).

[44] Nicholas A Lanzillo and Curt M Breneman, Journal of Physics: Condensed Matter **28**, 325502 (2016).

[45] C. A. McCoy, S. X. Hu, M. C. Marshall, D. N. Polsin, D. E. Fratanduono, Y. H. Ding, P. M. Celliers, T. R. Boehly, and D. D. Meyerhofer, Phys. Rev. B **102**, 184102 (2020).

[46] R. H. French *et al.*, AJC **60**, 251 (2007).

[47] Valentin V. Karasiev, James W. Dufty, and S. B. Trickey, Phys. Rev. Lett. **120**, 076401 (2018).